COmputatioNal Imaging as a training network for Smart biomedical dEvices

COmputatioNal Imaging as training network for Smart biomedical dEvices

Project No. 101072354

Deliverable 1.1

Software for simulation and reconstruction on compressed data

WP 1 – Advanced diffuse-optical tomography of biological tissues

Authors	Tanja Tarvainen (UEF), Meghdoot Mozumder (UEF), Andrea Farina (CNR), Aapo Perakorpi (DATRIX), Jarjish Rahaman (UEF), Matteo Bregonzio (DATRIX), Giovanna Tramontin (CNR)
Lead participant	CNR
Delivery date	29 November 2024
Dissemination level	Public
Type	Report

Version 1.0

Funded by the European Union

Engineering and Physical Sciences Research Council

Funded by the European Union (GA 101072354). Views and opinions expressed are however those of the author(s) only and do not necessarily reflect those of the European Union or the European Research Executive Agency. Neither the European Union nor the granting authority can be held responsible for them. UK participants are funded by UK Research and Innovation (UKRI) under the UK government's Horizon Europe funding guarantee grant number EP/X030733/1).

Revision history

Author(s)	Description	Date
Tanja Tarvainen (UEF), Meghdoot Mozumder (UEF), Andrea Farina (CNR), Aapo Perakorpi (DATRIX), Jarjish Rahaman (UEF), Matteo Bregonzio (DATRIX), Giovanna Tramontin (CNR)	Draft deliverable	21/11/2024
Jörn-Frederik Wotzlaw (accelCH)	Formal check and edits	28/11/2024
Andrea Farina (CNR)	Final version	29/11/2024

Contents

List of Figures **4**
Partner short names **4**
Abbreviations **4**
Executive summary **5**
Objectives 5
Methodology and Implementation 5
Outcomes 5
Next steps 5
1 Introduction **6**
2 Modelling and image reconstruction utilising temporal and spatial modulation **6**
2.1 Theory 6
2.1.1 Diffusion approximation 6
2.1.2 Structural patterns 7
2.1.3 Temporal frequencies 7
2.1.4 Image reconstruction 7
2.2 Simulations 7
2.2.1 Data generation 8
2.2.2 Image reconstruction 8
2.3 Results 8
2.3.1 Utilizing multiple temporal frequencies 8
2.3.2 Utilising multiple spatial patterns 9
2.4 Outcomes 9
3 Modelling with Monte Carlo methods and Machine-Learning Image reconstruction **9**
3.1 Monte Carlo method 9
3.1.1 Simulations with Monte Carlo 10
3.1.2 Data generation with Monte Carlo 11
3.1.3 Processing generated data 11
3.2 Image reconstruction 11
3.2.1 Model 12
3.2.2 Training 12
3.3 Results 12
4 Conclusions **12**
5 References **12**

List of Figures

Figure 1. (a) An example of a Hadamard Pattern, and its (b) 3D projection onto a simulated phantom. 7
Figure 2. Reconstructed images of cylindrical phantoms using Hadamard patterns up to order $H_{Nh} = 8$. 8
Figure 3. Reconstructed images of cylindrical phantoms using 5 Fourier frequencies, ...9
Figure 4. Geometry of a MC simulation.. 10
Figure 5. Photon fluence on the output side of the sample. 10
Figure 6. Results of Monte Carlo simulated photon propagation.. 11
Figure 7. Reconstructed image with a neural network from simulated measurements...12

Partner short names

CNR	Consiglio Nazionale delle Ricerche
UEF	University of Eastern Finland
DATRIX	DATRIX Spa

Abbreviations

D	Deliverable
M	Month
WP	Work Package
DOT	Diffuse Optical Tomography
TD	Time-Domain
IRF	Instrumental Response Function
FE	Finite-element
FEM	Finite-element method
ML	Machine Learning
MC	Monte Carlo

Executive summary

Deliverable D1.1 is part of Work Package 1 (“Advanced Diffuse Optical Tomography for Biological Tissues”) of the CONcISE project and provides a report on the methods developed for simulating the forward problem and managing the image reconstruction. These methods will be used for the analysis of the data acquired through the experimental system installed at CNR reported in D.1.2.

Objectives

The objective of this deliverable is to provide a software for simulation and image reconstruction of compressed time-domain diffuse optical tomography (TD-DOT) data. This involves:

- Simulation of TD-DOT data and implementation of compression using spatial and temporal modulation.
- Development and implementation of image reconstruction algorithms based on a classical inverse-problem approach and through machine-learning algorithms.

Methodology and Implementation

The main methodology is to implement a temporal and spatial modulation of time-domain data for modelling and image reconstruction in TD-DOT. The generation of forward time-domain profiles to simulate experimental data has been developed using the open-source Finite-Element Method (FEM) Toast++ (Schweiger 2014) and the open-source Monte Carlo Extreme (mcx) software (Fang 2019). These software were firstly adapted to accommodate Hadamard spatial illumination and detection and then used to simulate experimental measurements.

UEF leads the reconstruction approach using a truncated Fourier series representation of the data developed in a Bayesian framework, while DATRIX leads the reconstruction approach based on the training of a custom convolutional neural network starting from Monte Carlo (MC) data, which is intrinsically more accurate but slower than the FEM method.

In line with the concept of the CONcISE project, the 3 Doctoral Candidiates Giovanna Tarmontin Carneiro (DC1), Jarjish Rahaman (DC2) and Aapo Perakorpi (DC3) collaborated at this work. Initially, DC1 and DC3 adapted the open-source Mesh-based MC to work with both structured illumination and compressed sensing detection. Then, DC3 used the adapted MC to generate simulated data for training a convolutional neural network. Contemporarily, DC2 developed the forward and inverse problem @UEF and, during his recent secondment @CNR (September/October 2024) worked on matching the model to the experimental setup by also including the Instrumental Response Function (IRF) in the simulated data.

Outcomes

It was found that using a classical inverse problem approach under a Bayesian framework, spatial and temporal modulation can be used to compress time-domain DOT data, maintain the rich information in the data and provide good contrast in reconstructed images.

It was also found that using ML with MC simulated data it is possible to get a good localisation and reconstruction of the 3D absorption profile inside the sample.

Next steps

The algorithms developed will be used for analyzing the experimental data acquired through the platform developed by DC1 @CNR. Preliminary data was acquired during the secondment @CNR of DC2 to test the algorithm developed by UEF.

Further data will be acquired for the ML-based approach during the planned secondment @CNR of DC3.

Elaborate a strategy to further reduce the number of acquisitions without losing information.

1 Introduction

Diffuse Optical Tomography (DOT) is a non-invasive imaging technique to study biological tissue using visible and near-infrared light. Its applications in medical imaging range from functional brain studies to breast cancer imaging, small animal imaging, and tissue oxygenation monitoring (Arridge 1999, Gibson 2005). Time-domain diffuse optical tomography (TD-DOT) utilizes pulsed laser light to illuminate tissues and measure the time-varying temporal point spread function of the boundary exitance. Time-domain data is richer in information compared to other DOT systems that operate either using continuous wave or intensity illuminated light. However, modelling and image reconstruction in time-domain as such is inevitably computationally too expensive. Therefore, several reconstruction techniques have been developed in TD-DOT, that reduce the data using, for example, temporal moments or different data transforms (Schweiger 1999, Mozumder 2020). The use of temporal moments and data transforms in TD-DOT offers reduced computation time and memory by compressing the time-resolved data. However, to maintain the rich information of the time-domain systems and enable computationally reasonable modelling, novel methodologies need to be developed. One approach is to utilise structural illuminations and detection to enable data compression without information loss. Structural illumination and detection involve spatial manipulation of light projected onto the target tissue surface and detection of spatially modulated light signals. The use of structural illumination patterns helps to probe the imaging target using varying spatial frequencies and the structural detection compresses the measurements, by measuring specific spatial frequencies, reducing the size of the data. The technique has been utilized in DOT, TD-DOT and fluorescence DOT (Farina 2017). In this project, a software for modelling and imaging methodologies for TD-DOT is developed for compressed data, i.e. time-domain DOT data that is compressed both in spatially and in time but maintains the rich information.

Machine learning (ML) has become a valuable tool in DOT, addressing the challenges of its ill-posed inverse problem. Traditional methods rely on iterative algorithms, which often struggle to balance accuracy and computational efficiency. ML offers a data-driven approach to directly map boundary light measurements to internal optical properties, capturing difficult to analytically model non-linear relationships. While most of the work in the ML field focused on DOT has been applied to the iterative approaches by focusing individual steps during reconstruction (Yoo 2020, Mozumder 2022), some recent studies have proposed direct reconstruction using ML (Dale 2024). These direct reconstruction methods give us high speed (sub second) reconstruction times, and this is the approach we have also selected.

In the following, the two approaches will be discussed in detail.

2 Modelling and image reconstruction utilising temporal and spatial modulation

2.1 Theory

2.1.1 Diffusion approximation

In a typical TD-DOT measurement setup, near-infrared light is introduced into an object from its boundary. In this work, we consider the light transport model for TD-DOT as the diffusion approximation to the time-domain radiative transport equation (Arridge 1999, Ishimaru 1977). The interaction of light at the domain boundary is described by the Robin boundary condition (Arridge 1999). The solution of this model is numerically approximated using the finite element (FE) method. The FE-approximation of the time-domain diffusion approximation and the Robin boundary condition is implemented as described in (Mozumder 2020) with the time-stepping implemented with a Crank–Nicholson scheme. The discretized time-domain observation model is written as

$$y = A_t(\mu_a, \mu_s')$$

where A_t denotes the FE solution, y is the time-domain measurement data, μ_a and μ_s' are the discretized optical absorption and (reduced) scattering coefficients.

2.1.2 Structural patterns

Structural illumination and detection in DOT involve projecting light onto the tissue surface and measuring the resulting exitance using certain specific, pre-defined patterns. Earlier, various wavelet and Hadamard patterns have been proposed for use in DOT (Farina 2017). In this work, we studied the use of Hadamard patterns, due to their orthogonality and balanced distribution of elements. Figure 1 illustrates an example of a Hadamard matrix and the projection of the matrix on a 3D cylinder. When considering light illumination and detection, the negative entries of the Hadamard matrix are replaced with zeros, since light intensity is a non-negative phenomenon. Subsequently, the sources and detectors are modified in the diffusion approximation, to model source and detector Hadamard patterns up to a chosen order of matrices.

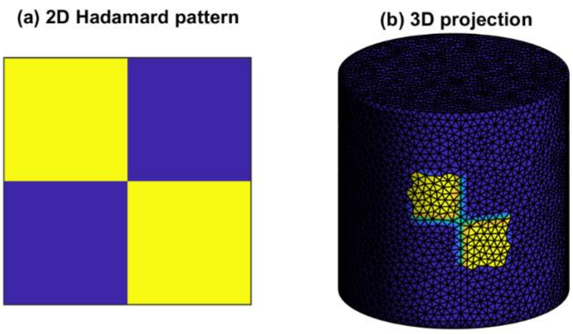

Figure 1. (a) An example of a Hadamard Pattern, and its (b) 3D projection onto a simulated phantom.

2.1.3 Temporal frequencies

Using the relationship between the time and frequency domain light transport models, it is possible to convert the measured time domain data to the frequency domain and utilize one or more frequencies for image reconstruction (Mozumder 2020). In this approach, we write a truncated Fourier series approximation of the time-resolved boundary exitance. The measured data is written as a discretized frequency-domain observation model

$$y = A_\omega(\mu_a, \mu_s') + e$$

Where y is the measured and Fourier-transformed data at multiple Fourier frequencies, A_ω is the discretized forward operator corresponding to the frequency-domain diffusion approximation, and e is the additive noise in the measurements.

2.1.4 Image reconstruction

The image reconstruction of the absorption and scattering coefficients can be written as a minimization problem

$$\widehat{\{\mu_a\}}, \widehat{\{\mu_s'\}} = \arg\min_{\mu_a, \mu_s'} \left\{ \left| L_e(y - A_\omega(\mu_a, \mu_s')) \right|^2 + \left| L_{\mu_a}(\mu_a - \eta_{\mu_a}) \right|^2 + \left| L_{\mu_s}(\mu_s - \eta_{\mu_s'}) \right|^2 \right\}$$

Where L_e is the Cholesky decomposition of the inverse of the noise covariance matrix. Additionally, the functional includes terms representing prior information about the target, where η_{μ_a} and $\eta_{\mu_s'}$ denote the means, and L_{μ_a} and $L_{\mu_s'}$ represent the Cholesky decomposition of the covariance matrices of the prior for absorption and scattering, respectively. In our study, we used a Gaussian Ornstein-Uhlenbeck prior for constructing the prior covariance matrices, and we solved the minimisation problem utilizing a Gauss-Newton method (Mozumder 2020).

2.2 Simulations

An open source software Toast++ (github.com/toastpp) was used in the FE-solution of the diffusion equation, projecting the Hadamard patterns, and implementation of the image reconstruction algorithms such as construction of the Jacobian matrices. It was run using MATLAB (R2022b, Mathworks, Natick, MA). The simulations were run on a Rocky Linux server equipped with an AMD EPYC Milan processor (2.2 GHz, 112 cores) and 693 GiB of RAM.

2.2.1 Data generation

In this work we utilized a cylinder with a radius of 25 mm and height 50 mm, shown in Figure 1 (b). We analyzed a target with background optical properties of μ_a= 0.01 mm^{-1} and μ_s'= 1 mm^{-1}. This target contained two absorption inclusions with μ_a = 0.02 mm^{-1} and two scattering inclusions with μ_s' = 2 mm^{-1}, as shown in the first column of Fig. 2. As shown, for both absorption and scattering, one inclusion was located near the object boundary and the other was located deeper in the domain.

For the simulated target, time-resolved data was generated using FE-approximation of the diffusion equation, in a mesh comprising 11744 nodes and 56222 tetraheadral elements. The time discretisation was set at 1 pico-second (ps). We used source pulses of 10 ps duration and our simulations had a temporal range of 10000ps. We simulated data utilising Hadamard illumination and detection patterns, using Hadamard matrices up to order 8. The Fourier transformed data were computed from the simulated time-resolved measurements. Random measurement noise e drawn from a zero-mean Gaussian distribution, where the standard deviations were specified as 1 % of the simulated noise-free measurement data, was added to the Fourier transformed (frequency domain) data at 1-5 Fourier frequencies.

2.2.2 Image reconstruction

To compute the estimates, we employed a finite element (FE) mesh consisting of 10780 nodes and 51542 elements. For the computation of the estimates, we assumed known noise mean and covariance. We conducted the following studies and evaluated their impact on estimation accuracy

- Impact of the number of Fourier frequencies
- Impact of the order of Hadamard patterns

2.3 Results

2.3.1 Utilizing multiple temporal frequencies

The MAP estimates obtained by using multiple Fourier frequencies are shown in Figure 2. As it can be seen, the estimates show improvements visually, and the relative error decreases, as the number of Fourier frequencies increase. However, the improvement plateaus beyond three or four frequencies, with no significant changes in image quality and relative errors with the addition of Fourier frequencies. This is consistent with previous DOT studies that reported that a few data transforms are sufficient for reasonable reconstructions in the case of uniform illuminations (Mozumder 2020, Schweiger 1999).

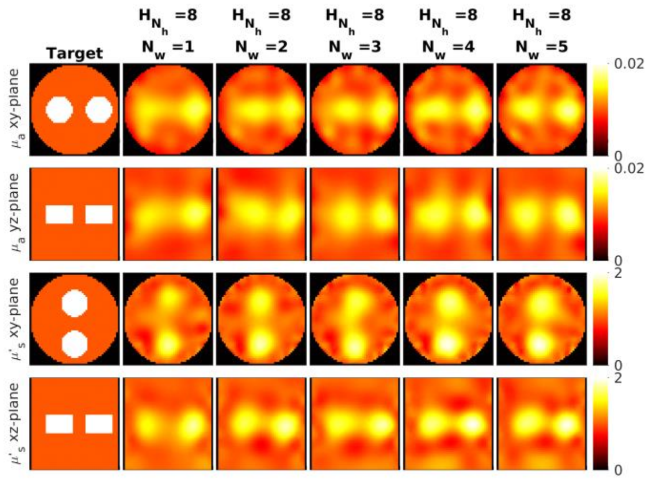

Figure 2. Reconstructed images of cylindrical phantoms using different number of Fourier frequencies (N_w) = 1, . . ., 5 and using Hadamard patterns up to order H_{Nh} = 8. Target optical parameters along the xy and yz planes of absorption (top two rows) and scattering (bottom two rows) are shown in the first column. The reconstructed images along the same planes, using 1-5 Fourier frequencies are shown in the second to sixth columns.

2.3.2 Utilising multiple spatial patterns

The MAP estimates obtained using Hadamard patterns of orders 2, 4, and 8, using five Fourier frequencies, are shown in **Figure 3**. The results show that the use of higher-order Hadamard patterns enhances the reconstruction quality both in terms of contrast and locating inclusion boundaries. The increased order of Hadamard patterns allows for a more detailed encoding of the spatial information, leading to enhanced reconstruction accuracy.

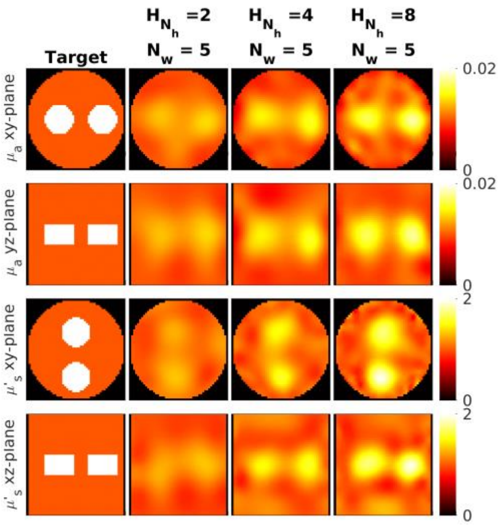

Figure 3. Reconstructed images of cylindrical phantoms using 5 Fourier frequencies, and using Hadamard orders (H_{Nh}) = 2, 4, and 8. Target optical parameters along the xy and yz planes of absorption (top two rows) and scattering (bottom two rows) are shown in the first column. The reconstructed images along the same planes, using 2-8 Hadamard orders are shown in the second to fourth columns.

2.4 Outcomes

Spatial and temporal modulation for modelling and image reconstruction of TD-DOT data was developed and implemented using an open access Toast++ software. The methodology was evaluated using numerical simulations that demonstrated that time-domain DOT data can be computationally efficiently handled using the proposed methodology, and that it can provide good quality reconstructions of absorption and scattering. It was seen that, increasing the number of Fourier frequencies to approximate time-domain data improves image quality up to an optimal point, beyond which additional frequencies offer minimal benefit. Furthermore, it was noticed, that utilising higher-order Hadamard patterns improves reconstructions. A manuscript of the results is in preparation.

3 Modelling with Monte Carlo methods and Machine-Learning Image reconstruction

3.1 Monte Carlo method

In this work, we consider the light transport model for TD-DOT using Monte Carlo (MC) simulations to solve the time-domain radiative transport equation. The MC method models the stochastic behaviour of photon propagation, including scattering and absorption events, by simulating the trajectories of individual photons as they interact with the medium. These methods have the advantage of solving the Radiative Transfer Equation (RTE), without approximation, for any geometries and optical properties combinations, but the drawback of providing noisy results and long computational time depending on the number og photon simulated. In the last decade, thanks to the computational power brought by the Graphical Processing Units (GPUs), those methods have become so fast that they can be used either for massive forward solvers but also in inverse problems.

3.1.1 Simulations with Monte Carlo

For simulating the photon propagation an open-source software Monte Carlo Extreme (Fang 2019) was used. Specifically, the mesh-based version (MMC) integrated with MATLAB (R2023b, Mathworks, Natick, MA) was run to generate the data. This version is openly available at: (https://github.com/fangq/mmc). DC1 and DC3 collaborated in adapting the code to work with structured illumination and single-pixel detection. This work will also serve as forward solver for the work in WP2 about illumination with Fourier patterns and for further validation of the methods reported in 2.

The simulation of light transport in diffuse media using the MMC code provides the most accurate solution of th photon transport to the radiative transfer equation (RTE). The adapted code enables Monte Carlo (MC) simulations for a wide range of illumination and detection patterns applied to the sample. Moreover, it allows the generation of samples with various shapes, including multiple inclusions positioned differently. Each part of the sample can be assigned specific absorption and scattering coefficients, as well as anisotropy coefficient g and refractive index n. The areas of illumination and detection within the simulation are also customisable by the user.

One example of a MC simulation is shown in **Figure 4**. **Figure 4**a) shows the sample with a cylindrical inclusion inside. Figure 4 b) shows the source and the direction of the illumination, while Figure 4 c) shows the detector on the opposite side.

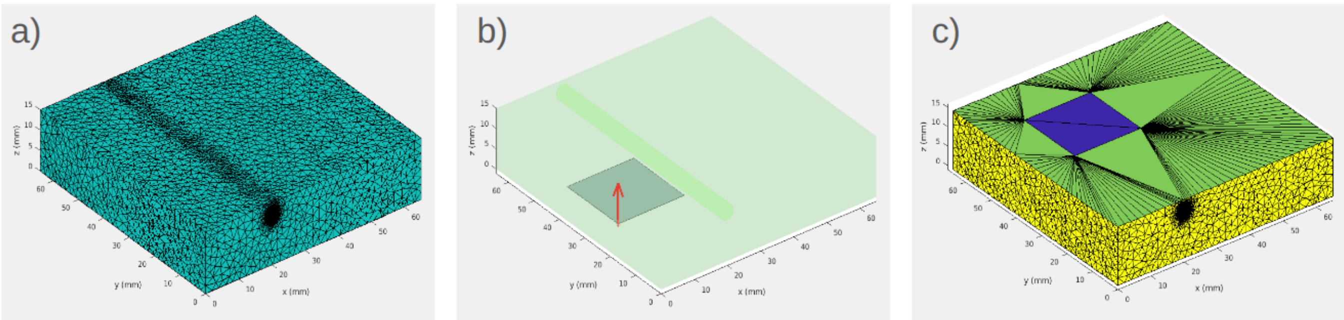

Figure 4. Geometry of a MC simulation. a) represents the sample with a cylindrical inclusion inside, b) shows the source and the direction of the illumination, and c), the detector on the opposite side.

Some of the outputs that can be acquired from the example simulation illustrated above are: the probability of finding the photon at a specific location and time (time resolved simulation), the number of scattering events per photon detected, entering and exiting position per photon in the medium, scattering angle per photon and photon fluence per mesh element. **Figure 5** shows the fluence on the output side of the sample when it is illuminated with a flat uniform pattern and with a Fourier pattern.

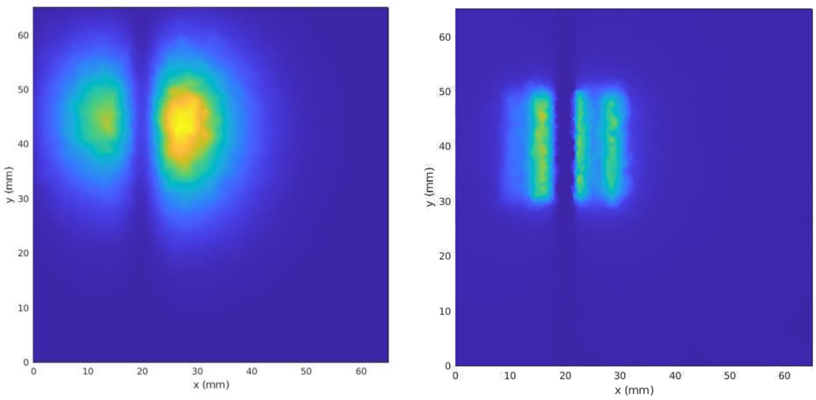

Figure 5. Photon fluence on the output side of the sample when it is illuminated with a flat uniform pattern (left image) and with a Fourier pattern (right image) using the simulation geometry showed in Figure 4.

For a homogeneous sample (without any inclusion), illuminated with a flat pattern, it is possible to obtain the results displayed in Figure 6. The image on the left shows the photon fluence at the detector, while the image on the right shows a histogram of the photon time flight from the source to the detector.

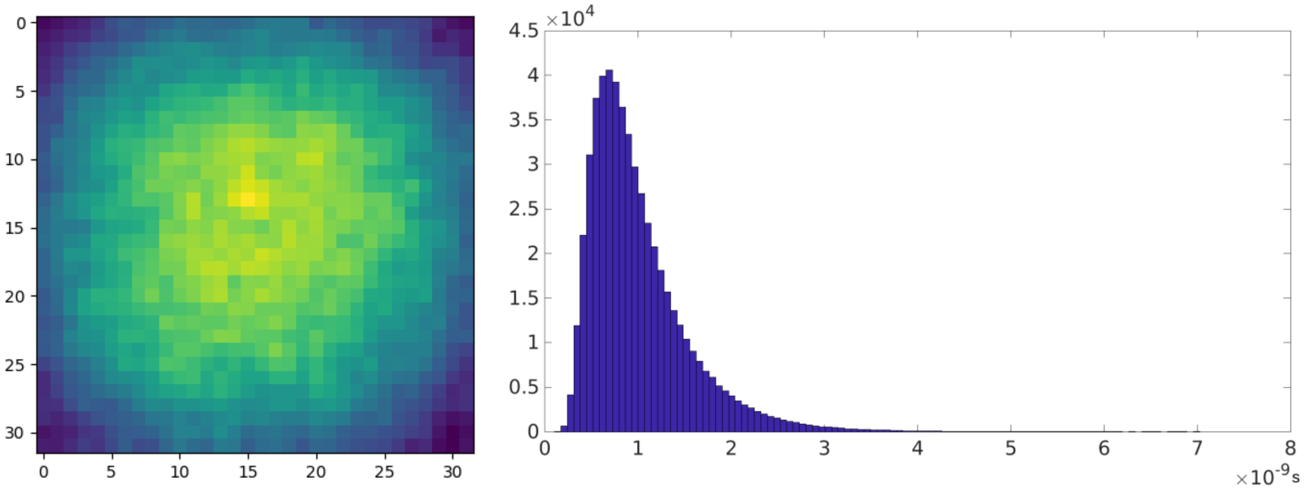

Figure 6. Results of Monte Carlo simulated photon propagation. Left: resulting measurement of light intensity distribution at the detector with flat uniform illumination. Right: resulting photon flight time distribution of photons from source to detector.

3.1.2 Data generation with Monte Carlo

For the purposes of training a robust Machine Learning model a diverse dataset was generated. Workflow was as follows: 1. different geometries were created as 3D meshes with varying sizes, orientations and optical properties (absorption and scattering). These geometries included: Spheres, cubes, pyramids and cylinders. The geometries were then embedded into a background mesh representing a 65x65x15 mm^3 slab. The optical properties of the slab and the embedded geometries/inclusions ranged from reduced-scattering of 0.5 to 1.5 mm^{-1} and absorption of 0.005 to 0.015 mm^{-1}. In total 6000 geometries were generated. 2. MMC was ran on (NVIDIA GeForce RTX 3050) for each of these geometries to generate photon propagation data of 10^8 photons. 3. Based on the flight-time, detection position and origin source the photons were binned in three different categories: Source bin (1024), detection bin (32x32), detection time bin (10).

3.1.3 Processing generated data

The noise arising from relatively low photon count during the Monte Carlo simulations was alleviated by applying a gaussian blur to each source bin separately. The Hadamard patterns were generated by summing up the photon counts along the corresponding source bins. These were used as the input to the neural network.

The volume of the reconstruction was on the 32 by 32 mm^2 area where the Hadamard patterns were projected. The mesh inside this volume was transformed into 64x64x30 voxel space with channels for the optical properties as well as a binary mask for the inclusion location. These were used as the target to the neural network.

Finally these were .mat files were converted into .zarr files and moved onto Datrix SpA servers in Milan for the network training.

3.2 Image reconstruction

The neural network was designed to reconstruct a 3D voxel structure of size 64x64x30 with 3 channels: absorption coefficient, scattering coefficient and binary, mask for the inclusion. The model did this based on an input of 10240 images (size 32 by 32) of light intensity distributions. These images from a single sample differed in two ways: each sample had 10 different timesteps and 1024 different Hadamard illumination patterns. The goal of the image reconstruction with just a neural network was to ascertain whether it is feasible and if it has advantages over more traditional methodologies, such as speed.

3.2.1 Model

The neural network model was built with PyTorch and in total had ~200 million parameters. The encoder included 2D convolutions for analysing the 32by32 image images, gated recurrent unit for time domain and 1D convolutions for the Hadamard pattern dimension. For the decoder part 3D convolutions were used to up sample back to the 3D structure from the extracted features. For activations we used leakyReLU and used also Batchnorm, Maxpooling, Dropout of 0.3.

3.2.2 Training

For training the model a Nvidia L40S GPU was utilized. The training was done using optimizer Adam with a learning rate of 0.0001 and loss function was a combination of binary cross entropy, mean squared entropy and total variation. The model was trained for 100 epochs with validation split of 0.2.

3.3 Results

As of writing, the precision of the model stands around 80% e.g. True positives / (False positives + False negatives) is around 0.8 across the dataset. The binary mask predicting the inclusion location is more accurate and has less noise as well as artifacting than the other two channels (absorption and scattering coefficients) which predict continuous real values instead of binary ones. The model is fast and able to reconstruct the 3D distribution of the variables in 0.25 seconds.

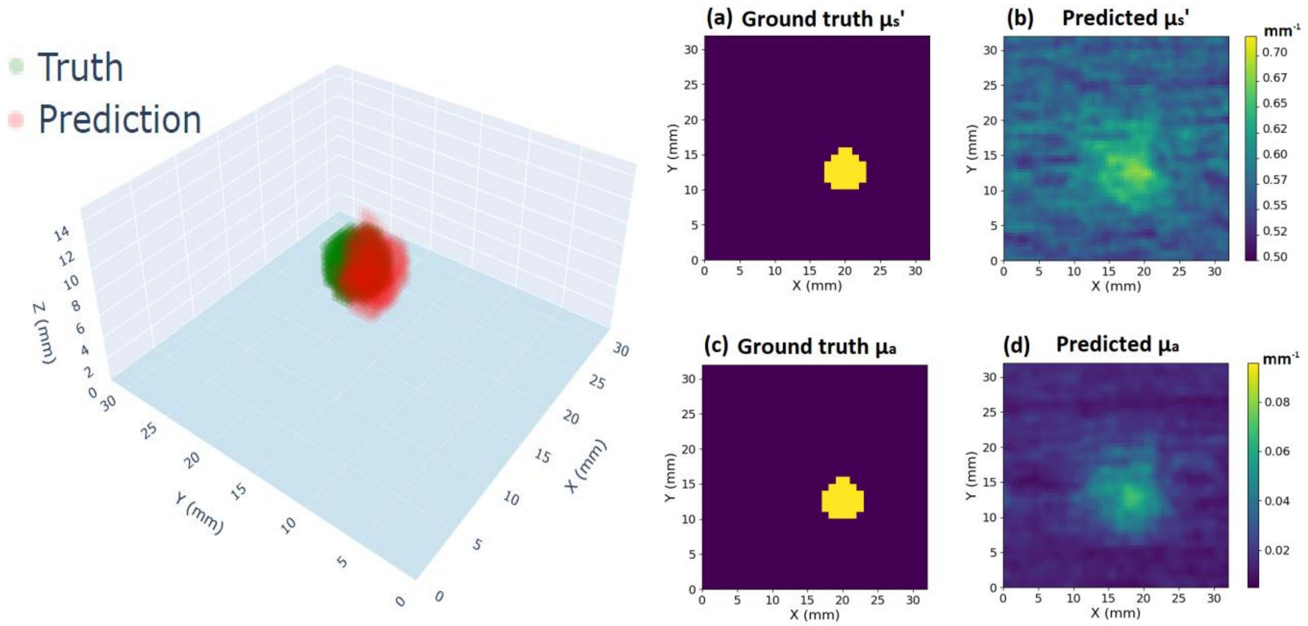

Figure 7. Reconstructed image with a neural network from simulated measurements of a spherical inclusion with differing optical properties compared to the background. On the left there is a 3D representation of a thresholded (at 0.5) binary mask of the predicted voxels (red) vs true location of the inclusion (green). On the right there are predicted optical properties of an x-y slice of the slab vs. actual values. a) shows the reduced scattering and b) shows the absorption.

4 Conclusions

A software platform managing different forward solvers for the light propagation in biological tissues has been developed together with different modalities of image reconstruction from data gather using spatial light modulation and single-pixel detection in time-domain.

5 References

Arridge, S. R. (1999). Optical tomography in medical imaging. Inverse Problems, 15(2).

Dale, R., Zheng, B., Orihuela, F., Ross, N., O'Sullivan, T. Howard, S., & Dehghani, H (2024). Deep learning-enabled high-speed, multi-parameter diffuse optical tomography. Journal of Biomedical Optics, 29(7), 076004.

Fang, Q., & Yan, S. (2019). Graphics processing unit-accelerated mesh-based Monte Carlo photon transport simulations. Journal of Biomedical Optics, 24(11), 115002.

Farina, A., Betcke, M., di Sieno, L., Bassi, A., Ducros, N., Pifferi, A., … D'Andrea, C. (2017). Multiple-view diffuse optical tomography system based on time-domain compressive measurements. Optics Letters, 42(14), 2822.

Gibson, A. P., Hebden, J. C., & Arridge, S. R. (2005). Recent advances in diffuse optical imaging. Physics in Medicine and Biology, 50(4).

Ishimaru, A. (1977). Wave propagation and scattering in random media. New York: Academic Press.

Mozumder, M., Hauptmann, A., & Tarvainen, T. (2022). A Model-Based Iterative Learning Approach for Diffuse Optical Tomography. IEEE Trans Med Imaging 41(5):1289-1299.

Mozumder, M., & Tarvainen, T. (2020). Time-domain diffuse optical tomography utilizing truncated Fourier series approximation. Journal of the Optical Society of America A, 37(2), 182.

Schweiger, M., & Arridge, S. R. (1999). Application of temporal filters to time resolved data in optical tomography. Physics in Medicine and Biology, 44(7), 1699–1717.

Schweiger, M. & Arridge, S. (2014). The Toast ++ software suite for forward and inverse modelling in optical tomography. J. Biomed. Opt. **19**, 1–15.

Yoo J, Sabir S, Heo D, Kim KH, Wahab A, … Ye JC. (2020). Deep Learning Diffuse Optical Tomography. IEEE Trans Med Imaging. Apr;39(4):877-887.